On approaching the ultimate limits of communication using a photon-counting detector

Baris I. Erkmen, Bruce E. Moision, Samuel J. Dolinar, Kevin M. Birnbaum, and Dariush Divsalar

Jet Propulsion Laboratory, California Institute of Technology,
4800 Oak Grove Dr., Pasadena CA 91109, USA

ABSTRACT

Coherent states achieve the Holevo capacity of a pure-loss channel when paired with an optimal measurement, but a physical realization of this measurement scheme is as of yet unknown, and it is also likely to be of high complexity. In this paper, we focus on the photon-counting measurement and study the photon and dimensional efficiencies attainable with modulations over classical- and nonclassical-state alphabets. We analyze two binary-modulation architectures that improve upon the dimensional versus photon efficiency tradeoff achievable with the state-of-the-art coherent-state on-off keying modulation. We show that at high photon efficiency these architectures achieve an efficiency tradeoff that differs from the best possible tradeoff—determined by the Holevo capacity—by only a constant factor. The first architecture we analyze is a coherent-state transmitter that relies on feedback from the receiver to control the transmitted energy. The second architecture uses a single-photon number-state source.

1. INTRODUCTION

Because photons are fundamentally quantum mechanical, the ultimate limit of reliable communication using photons is determined by the Holevo capacity.[1] Although coherent states are known to achieve this capacity with an optimal measurement, such as the square-root measurement,[1–3] a physical apparatus that implements this measurement for bosonic communications is not yet known. What is known, however, is that standard measurements (e.g., photon-counting, homodyne, heterodyne) yield capacities that are bounded away from the ultimate Holevo capacity. Furthermore, receiver architectures that have the potential to surpass the state-of-the-art attainable with standard measurements, thus far, have required a steep increase in implementation complexity in return for a small performance improvement.[4–6]

This observation motivates our investigation, in this paper, of the ultimate limits achievable with a photon-counting receiver, when it is coupled with novel quantum-state alphabets and signaling architectures that are tailored to improve the information efficiency obtained with this measurement. Although the information capacity of photon counting is strictly bounded away from the Holevo capacity (except in the limit of zero loss[7]), our interest here is in characterizing the gap to the ultimate bound, and minimizing it by use of novel signaling architectures. In particular, we analyze two novel photon-counting architectures that offer performance improvements relative to the standard method of binary modulation of coherent-state amplitudes (standard on-off keyed communication). The first architecture is a coherent-state transmitter that relies on feedback from the receiver to shut off the transmitted pulse, once a photon is detected. The second architecture uses a binary modulation of vacuum and a single-photon number state. The former architecture can be interpreted as mimicking the photodetection statistics of a single-photon number state at the receiver, which is near-optimal when the mean photon number is much less than unity, or equivalently, when the photon efficiency is high. The latter architecture starts with a number-state modulation, but is sensitive to losses in the propagation path, so it approaches the Holevo capacity only in the near field wherein the transmitter-to-receiver coupling efficiency is high.

Our paper is organized as follows. Section 2 reviews some fundamentals of beam propagation in vacuum. In Section 3 we study the standard coherent-state on-off keying (OOK) plus ideal photon counting architecture, with emphasis on the best possible photon information effiency (PIE) versus dimensional information efficiency

Send correspondence to B.I.E. at baris.i.erkmen@jpl.nasa.gov.

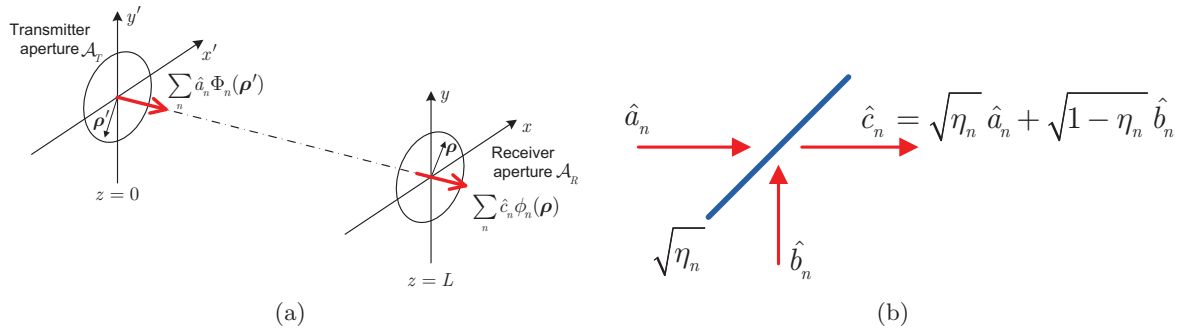

(a) (b)

Figure 1. The normal-mode decomposition for quasimonochromatic, paraxial free-space (i.e., vacuum) propagation. (a) The paraxial link geometry and propagation of eigenmodes, and (b) the beamsplitter representation of a single channel.

(DIE) tradeoff achievable with this scheme.[5,8] We show that the ratio of the DIE attained by standard OOK and that obtained by the optimal tradeoff (i.e., the Holevo bound) grows linearly with PIE for large values of PIE. In Section 4, we introduce our first novel communication architecture that improves upon this state of the art, assuming ideal feedback is present between the receiver and the transmitter. We derive the optimal PIE-DIE tradeoff attainable with this architecture, and compare it to both the ultimate (Holevo) bound and the standard OOK tradeoff curve. We show that at high PIE, the ratio of the DIE achieved with this architecture is a constant fraction of that predicted by the Holevo bound. In Section 5 we analyze our second architecture, which encodes information in the vacuum and the single-photon number state. Again, we show that the DIE is a constant fraction of the optimal DIE at high PIE values, with the fraction determined by the end-to-end channel loss. Finally, in Section 6, we conclude our manuscript with a discussion of the key implications of these results.

2. PRELIMINARIES

Here we review the formulation that converts free-space propagation into a set of beamsplitter channels. Quasimonochromatic, paraxial propagation in vacuum through finite transmitter and receiver apertures is represented by a linear superposition integral given by

$$\hat{E}_L(\boldsymbol{\rho}, t) = \int_{\mathcal{A}_T} h(\boldsymbol{\rho} - \boldsymbol{\rho}')\hat{E}_0(\boldsymbol{\rho}', t - L/c)\mathrm{d}\boldsymbol{\rho}' + \hat{\mathcal{L}}_v(\boldsymbol{\rho}, t)\,, \tag{1}$$

where $\hat{E}_0(\boldsymbol{\rho}, t)$ for $\boldsymbol{\rho} \in \mathcal{A}_T$ is the baseband envelope of a z-propagating $\sqrt{\text{photons/m}^2\text{s}}$-units quantum field operator transmitted from the $z = 0$ aperture, $\hat{E}_L(\boldsymbol{\rho}, t)$ for $\boldsymbol{\rho} \in \mathcal{A}_R$ is the corresponding quantum field operator received over the $z = L$ aperture, and $\hat{\mathcal{L}}_v(\boldsymbol{\rho}, t)$ is an auxiliary operator in its vacuum (i.e., unexcited) state needed to preserve the delta-function commutator brackets of the field operators.* The propagation kernel is the well-known Huygens-Fresnel Green's function from classical paraxial optics, namely

$$h(\boldsymbol{\rho} - \boldsymbol{\rho}') \equiv \frac{1}{i\lambda_0 L} e^{i2\pi L/\lambda_0} e^{i\pi|\boldsymbol{\rho}-\boldsymbol{\rho}'|^2/(\lambda_0 L)}\,. \tag{2}$$

Because paraxial propagation is a linear transformation of the input field, a singular-value decomposition can be carried out to represent the propagation as a set of parallel (orthogonal) pure-loss channels, as shown in Fig. 1.[9,10] This decomposition—also known as the normal-mode decomposition[9–11]—results in a set of input eigenfunctions, $\{\Phi_n(\boldsymbol{\rho}')\}$, that are complete and orthonormal over the input aperture $\boldsymbol{\rho}' \in \mathcal{A}_T$. Upon propagation to the receiver plane, each input eigenfunction $\Phi_n(\boldsymbol{\rho}')$ is transformed into a corresponding output eigenfunction $\phi_n(\boldsymbol{\rho})$—where $\{\phi_n(\boldsymbol{\rho})\}$ also collectively form a complete and orthonormal basis on the receiver aperture $\boldsymbol{\rho} \in \mathcal{A}_R$—and is attenuated by a less-than-unity singular-value $\sqrt{\eta_n}$ due to diffraction. The resultant propagation model

*The paraxial field operators satisfy $[\hat{E}_z(\boldsymbol{\rho}_1, t_1), \hat{E}_z^\dagger(\boldsymbol{\rho}_2, t_2)] = \delta(\boldsymbol{\rho}_1 - \boldsymbol{\rho}_2)\delta(t_1 - t_2)$ and $[\hat{E}_z(\boldsymbol{\rho}_1, t_1), \hat{E}_z(\boldsymbol{\rho}_2, t_2)] = 0$ for any $0 \le z \le L$.[9]

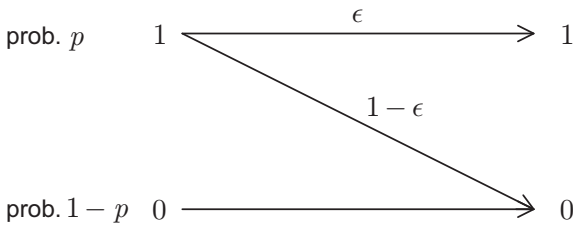

Figure 2. The input-output probability transition map for a Z channel with erasure probability $1-\epsilon$.

for the transmitter-plane field operator describing each input mode is therefore equivalent to that through a beamsplitter with photon-flux transmissivity η_n.[9]

An optical communication system's link geometry can be classified into two regimes, according to the distribution of the singular values of its normal-mode decomposition. In the *far field* regime there is only one eigenfunction (i.e., η_1) whose power coupling differs appreciably from 0. In contrast, in the *near field* regime multiple η_n's are close to unity. For paraxial propagation in vacuum, whether a particular link geometry is in the far field or near field is determined solely by comparing the Fresnel number product

$$D_F \equiv \frac{A_T A_R}{(\lambda_0 L)^2} = \sum_{n=1}^{\infty} \eta_n \tag{3}$$

to unity, with $D_F \ll 1$ corresponding to the *far field*, and $D_F \gg 1$ corresponding to the *near field*. In Eq. (3), A_T is the transmitter aperture area, A_R is that of the receiver aperture, λ_0 is the center wavelength of the optical field, and L is the distance between the transmitter and the receiver.

3. CONVENTIONAL ON-OFF KEYING (OOK) WITH COHERENT STATES

Now we focus on a single mode of these parallel channels, which is modelled as a beamsplitter with transmissivity η. We start with coherent-state on-off keying modulation paired with an ideal photon counting receiver, both to serve as a baseline for the architectures that will follow in future sections, and to introduce our analysis framework using a well-understood example.[12]

Consider a binary intensity-modulated optical channel, in which each channel use has a duration of T seconds. In one channel use we either receive a pulse with photon flux equal to λ (expressed in units of photons/sec) with probability p, or no pulse—i.e., a photon flux equal to 0—with probability $1-p$. This photon flux is incident on an ideal infinite-bandwidth photon-counting photodetector, which yields a Poisson point process with rate either λ or 0, depending on the transmitted symbol. Since detection of a single photon perfectly reveals the transmitted symbol, the channel output can be classified (with no loss of information) into binary outcomes: either no detection event occurs or at least one detection event occurs. Thus this channel is a Z-channel, illustrated in Fig. 2, where $\epsilon = 1 - e^{-\lambda T}$ is the probability that at least one photon is detected given that the incident photon flux is λ. The mutual information I^Z, in bits per channel use, is

$$I^Z = H_2(p\epsilon) - pH_2(\epsilon)\,, \tag{4}$$

where $H_2(x) = -x\log_2 x - (1-x)\log_2(1-x)$ is the binary entropy function. It will be convenient to express this mutual information as

$$I^Z = \bar{n}\left[h_2(\bar{n}) - h_2(\epsilon)\right]\,, \tag{5}$$

where $\bar{n} \equiv p\epsilon$ is the probability of detecting at least one photon, and $h_2(x) \equiv H_2(x)/x$ is the mean derivative of the binary entropy function between 0 and x.

Ideal coherent-state OOK (i.e., infinite-extinction-ratio binary amplitude modulation of a continuous-wave laser having a deterministic polarization state, a single transverse spatial mode, and a single longitudinal mode)

occupies approximately one signaling dimension, which we denote as $d^{\mathrm{OOK}} = 1$. This standard OOK modulation costs an average of

$$\bar{n}^{\mathrm{OOK}} = p\lambda T = -p\ln(1-\epsilon) = \bar{n}d(\epsilon) \tag{6}$$

photons per channel use, where $\bar{n}$ is defined above, and

$$d(\epsilon) \equiv \frac{-\ln(1-\epsilon)}{\epsilon} = \frac{\lambda T}{1-e^{-\lambda T}}\,. \tag{7}$$

Although the dimensionless quantity $d(\epsilon)$ is introduced in Eq. (6) as a matter of convenience, we shall see in the next section that it has a relevant physical interpretation. Combining Eqs. (5) and (6), we express the mutual information gained per (average) photon, in standard OOK, as

$$i_p^{\mathrm{OOK}} \equiv \frac{I^Z}{\bar{n}^{\mathrm{OOK}}} = \frac{h_2(\bar{n}) - h_2(\epsilon)}{d(\epsilon)} \quad \text{bits/photon.} \tag{8}$$

The corresponding mutual information per signal dimension is

$$i_d^{\mathrm{OOK}} \equiv \frac{I^Z}{d^{\mathrm{OOK}}} = \bar{n}\left[h_2(\bar{n}) - h_2(\epsilon)\right] = \bar{n}d(\epsilon)i_p^{\mathrm{OOK}} \quad \text{bits/dimension,} \tag{9}$$

or, equivalently,

$$i_d^{\mathrm{OOK}} = h_2^{-1}\Big(d(\epsilon)i_p^{\mathrm{OOK}} + h_2(\epsilon)\Big)i_p^{\mathrm{OOK}}d(\epsilon)\,, \tag{10}$$

where $h_2^{-1}(\cdot)$ is the inverse of the one-to-one mean-derivative function, $h_2(\cdot)$, introduced earlier in Eq. (5).

The convex hull of all attainable $(i_p^{\mathrm{OOK}}, i_d^{\mathrm{OOK}})$ pairs traces the best photon information efficiency (PIE) and dimensional information efficiency (DIE) tradeoff attainable with standard OOK. We state this formally as

$$c_d^{\mathrm{OOK}}(i_p) = \max_{\epsilon\in[0,1]|i_p^{\mathrm{OOK}}=i_p} i_d^{\mathrm{OOK}}(i_p^{\mathrm{OOK}}, \epsilon)\,, \tag{11}$$

where $c_d^{\mathrm{OOK}}(i_p)$ denotes the convex hull, and plot it in Fig. 3(a). It is qualitatively apparent from the plot that the PIE of this scheme is unbounded—albeit with vanishing DIE—and that while the PIE of standard OOK approaches that of the Holevo bound at high values of PIE, the gap between the two curves grows in the DIE axis. To quantify this gap we derive the large-PIE asymptotic form of the standard OOK tradeoff curve. We begin by noting that for $\bar{n} \ll 1$ (which corresponds to the large-PIE regime[12]), we have $h_2(\bar{n}) \approx \log_2(e/\bar{n})$, such that Eq. (10) is approximately

$$i_d^{\mathrm{OOK}}(i_p, \epsilon) \approx (ei_p 2^{-i_p})2^{-(d(\epsilon)-1)i_p}2^{-h_2(\epsilon)}d(\epsilon)\,. \tag{12}$$

In Eq. (12), $ei_p2^{-i_p}$ is the asymptotic formula (when $i_p \gg 1$) for the best possible variation of dimensional efficiency with photon efficiency, determined by the Holevo limit.[5,13] The next term, $2^{-(d(\epsilon)-1)i_p}$, is less than unity because $d(\epsilon) > 1$. So, any fixed ϵ results in i_d^{OOK} decreasing *exponentially* relative to the Holevo DIE, with increasing i_p. Therefore, the optimal ϵ must decrease towards 0 with increasing i_p, such that the product $(d(\epsilon)-1)i_p$ remains small as i_p grows without bound. To quantify this intuition, we write $d(\epsilon) \approx 1 + \epsilon/2$ and $2^{-h_2(\epsilon)} \approx \epsilon/e$, which holds for $\epsilon \ll 1$, and substitute them in Eq. (12) to obtain

$$i_d^{\mathrm{OOK}}(i_p, \epsilon) \approx i_p 2^{-i_p}2^{-\epsilon i_p/2}\epsilon(1+\epsilon/2)\,. \tag{13}$$

When we maximize this expression over ϵ for each i_p, we find that

$$\epsilon^*(i_p) \equiv \arg\max_{\epsilon\in[0,1]} i_d^{\mathrm{OOK}}(i_p, \epsilon) = 2\log_2 e\, i_p^{-1}(1 + \log_2 e\, i_p^{-1})\,, \tag{14}$$

and correspondingly,

$$\begin{aligned} c_d^{\mathrm{OOK}}(i_p) &\equiv i_d^{\mathrm{OOK}}(i_p, \epsilon^*) && (15)\\ &\approx (2\log_2 e/e)2^{-i_p}e^{-\log_2 e\, i_p^{-1}}(1+\log_2 e\, i_p^{-1})^2 && (16)\\ &\approx (2\log_2 e/e)2^{-i_p}(1+\log_2 e\, i_p^{-1}) && (17)\\ &\approx (2\log_2 e/e)2^{-i_p}\,. && (18) \end{aligned}$$

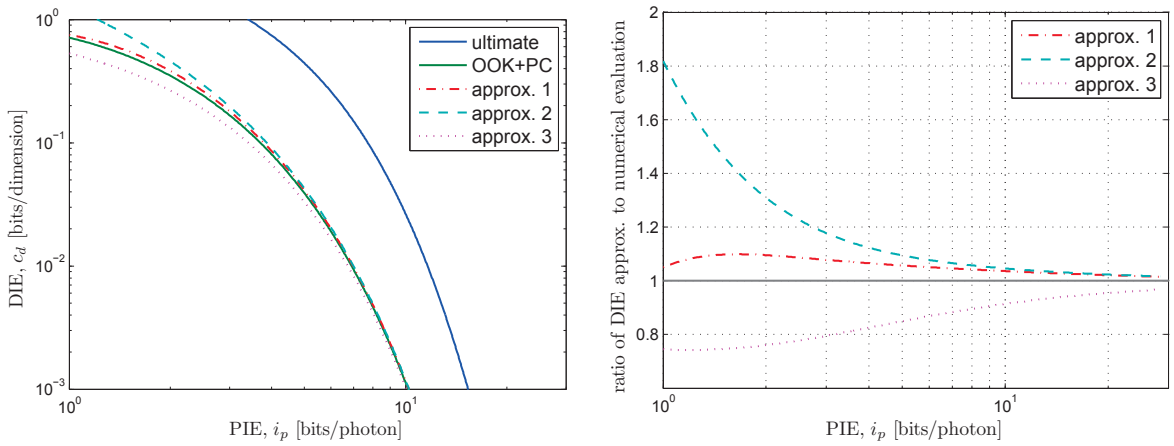

(a) (b)

Figure 3. Asymptotic approximations for the dimensional information efficiency (DIE), c_d, and the numerically-evaluated DIE curve for on-off keying with ideal photon counting (OOK+PC) are plotted. (a) The numerically-evaluated PIE versus DIE tradeoff curve and three asymptotic approximations. (b) The ratio of the approximations to the numerically-evaluated DIE. The most accurate approximation (approx. 1) is given in Eq. (16), the second best approximation (approx. 2) is given in Eq. (17), and finally, the simplest expression (approx. 3) is given in Eq. (18).

Eqs. (16)–(18) demonstrate a succession of approximations which are plotted along with the numerically-evaluated DIE curve in Fig. 3(a). In addition, the ratios of these approximations to the numerically-evaluated DIE are plotted in Fig. 3(b). Eq. (16) is the most accurate of the three approximations, and follows the numerically-evaluated DIE curve fairly well at all PIE values. From the plots we determine that the approximation is within 6% of the numerical DIE for $i_p > 5$ bits/photon. The Eq. (17) simplification eliminates the exponential term in the previous expression using the fact that $i_p \gg 1$. It achieves better than 6% accuracy when $i_p > 8$ bits/photon. Finally, when $i_p > 16$ bits/photon, the Eq. (18) approximation, which is also the simplest, achieves better than 6% accuracy. This last asymptotic approximation is *equal* to the asymptotic formula for pulse-position modulation (PPM) and ideal photon counting,[5] confirming the well-known result that the PIE-DIE tradeoff for PPM and OOK converge for sufficiently large PIE.

We close this section with a comparison of the DIE achievable with standard OOK to the highest theoretically achievable DIE (with an isotropic Gaussian distribution on a coherent-state modulation alphabet and the optimal quantum measurement) given by the Holevo bound. As indicated above, the Holevo bound yields an asymptotic form for the DIE, for $i_p \gg 1$, as $c_d^{\mathrm{Hol}} = e i_p 2^{-i_p}$ bits/dimension,[5,13] which implies that asymptotically

$$\frac{c_d^{\mathrm{Hol}}(i_p)}{c_d^{\mathrm{OOK}}(i_p)} = \frac{e^2}{2\log_2 e} i_p = 2.561 i_p \,. \tag{19}$$

Therefore, for high PIE values, standard OOK achieves a DIE that has *suboptimal* parametric dependence on PIE, relative to the optimal tradeoff predicted by the Holevo bound. In particular, the gap between the optimal DIE and that achieved by standard OOK grows linearly with increasing PIE.

4. OOK WITH SINGLE-PHOTON SHUTOFF

As implied by the analysis above, in coherent-state OOK with ideal photon counting, the detection of a single photon is sufficient to perfectly resolve the transmitted symbol. Any additional photodetection events do not convey information. Thus, the transmitter could conserve resources by turning the transmitted pulse off if it were informed of the first photodetection event at the receiver. Consider the modified—and idealized—receiver structure illustrated in Fig. 4, in which the receiver provides delay- and noise-free feedback to the transmitter, informing it to terminate the transmitted pulse as soon as the first photon is detected. If no photons are detected, either because vacuum was transmitted or because an erasure event occurred, the receiver waits until the end of

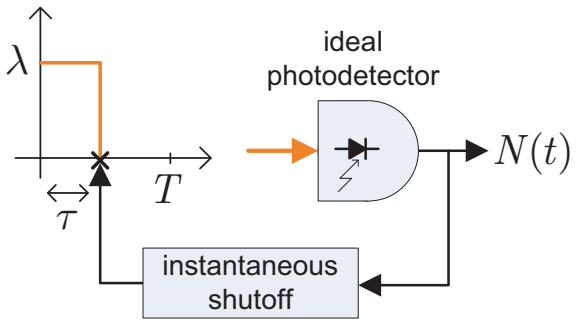

Figure 4. An ideal single-photon shutoff receiver, with feedback to the transmitter.

the T-second window and then restarts anew. We refer to this system as *OOK with single-photon shutoff* and use the shorthand notation 1S in referring to its variables in the following analysis.

For this receiver architecture, the input-output channel map is still equivalent to the Fig. 2 Z channel. Thus, the mutual information between the input and output is again given by the expression in Eq. (5), but now the mean photon number per channel use has been reduced to

$$\bar{n}^{1\mathrm{S}} = p\lambda E[\tau] = p(1 - e^{-\lambda T}) = \bar{n} = \frac{\bar{n}^{\mathrm{OOK}}}{d(\epsilon)}\,. \tag{20}$$

Here, τ is the random variable that denotes the duration of the pulse (given one is transmitted), $\bar{n}^{\mathrm{OOK}}$ is the mean photon number for standard OOK given in Eq. (6), and $d(\epsilon)$ is defined in Eq. (7). Because $d(\epsilon) > 1$, for the same channel transition probability ϵ and the same channel input probability p (i.e., the same input-output mutual information I^Z), the system with single-photon shutoff requires fewer photons—on average—by a factor $d(\epsilon)$, compared to the conventional OOK system with no feedback.[†]

The OOK single-photon shutoff system achieves its improved photon efficiency at a price of requiring additional resources for the feedback channel and increased bandwidth usage on the forward (optical) link. Here we limit our focus to the bandwidth increase in the forward link, which is due to shortened pulse durations when transmission is shut off before the full T seconds of the nominal signaling interval. Because the pulse transmission consists of probabilistic pulses of random duration in every T-second window, the power spectral density of the optical pulse train is not trivial to evaluate. Nonetheless, it is reasonable to expect that at high mean photon number per pulse ($\lambda T \gg 1$) the bandwidth occupancy is the reciprocal of the mean time to the first photon arrival λ, whereas at low mean photon number per pulse ($\lambda T \ll 1$) the bandwidth usage is approximately $1/T$. We use the reciprocal of the average duration of a transmitted pulse, i.e., $1/E[\tau] = \lambda/(1 - e^{-\lambda T})$ as the bandwidth of the random process resulting from our single-photon shutoff OOK scheme. In the appendix, we derive the precise power spectral density of this random process and show that this definition encompasses 90% of the mean photon flux.[‡] Following our bandwidth definition, the number of temporal dimensions per channel use—determined by the time-bandwidth product—is given by

$$d^{1\mathrm{S}} = \frac{\lambda T}{1 - e^{-\lambda T}} = \frac{-\ln(1-\epsilon)}{\epsilon} = d(\epsilon)\,, \tag{21}$$

i.e., $d(\epsilon)$, which was introduced in Eq. (6) for convenience, corresponds to the number of temporal dimensions occupied by the OOK single-photon shutoff system.

We can now write the mutual information per photon as

$$i_p^{1\mathrm{S}} = h_2(\bar{n}) - h_2(\epsilon) \quad \text{bits/photon}, \tag{22}$$

[†]Note that $\bar{n}^{1\mathrm{S}}$ is equal to $\bar{n}$, the probability of detecting at least one photon, which we had introduced earlier to conveniently express the mutual information for the Z channel.

[‡]It is also the case that for conventional OOK with pulse duration T, 90% of the mean photon flux is concentrated in a frequency bandwidth of $1/T$. Therefore, using $1/E[\tau]$ for the bandwidth of the single-photon shutoff scheme offers a fair comparison to conventional OOK.

and the corresponding mutual information per dimension as

$$i_d^{1S} = \frac{\bar{n}}{d(\epsilon)} \left[h_2(\bar{n}) - h_2(\epsilon) \right] = \frac{\bar{n}}{d(\epsilon)} i_p^{1S} \quad \text{bits/dimension.} \tag{23}$$

Comparing these expressions to the corresponding ones for standard OOK—given in Eqs. (8) and (9) respectively–we arrive at the following ratio equality:

$$\frac{i_d^{OOK}}{i_d^{1S}} = \frac{i_p^{1S}}{i_p^{OOK}} = d(\epsilon)\,, \tag{24}$$

i.e., for the same channel transition probability ϵ and input probability p, the modified OOK system with single-photon shutoff has better photon efficiency by a factor of $d(\epsilon)$ and worse dimensional efficiency by the same factor, in comparison to standard OOK. This is a favorable tradeoff when the log-domain curve defined by the pair of points $(\log_2 i_p^{OOK}, \log_2 i_d^{OOK})$ has slope less than -1. Returning to the Eq. (12) approximation to standard OOK's mutual information per dimension, we evaluate that this slope shift occurs approximately at

$$i_p^* \approx 2 \log_2 e / d(\epsilon) < 2 \log_2 e\,. \tag{25}$$

Thus, for moderately-high photon efficiency (specifically, when $i_p > 2 \log_2 e \approx 2.885$ bits/photon) the single-photon shutoff offers a favorable tradeoff between bits per photon and bits per dimension for any fixed ϵ value.

Each feasible value of the pair $(\bar{n}, \epsilon)$ corresponds to a point in the $(i_p^{1S},\, i_d^{1S})$ plane, and the convex hull of these points determine the best achievable tradeoff between PIE and DIE with this system. In order to compute this convex hull we write i_d^{1S} as a function of i_p^{1S} and ϵ by eliminating the variable $\bar{n}$, then maximize over ϵ. The first step of this process yields

$$i_d^{1S}(i_p, \epsilon) = h_2^{-1}\big(i_p + h_2(\epsilon)\big) i_p / d(\epsilon)\,, \tag{26}$$

where we have dropped the 1S superscript from i_p to avoid notation clutter, and we have explicitly defined i_d^{1S} as a function of the variables i_p and ϵ. The DIE attainable with this single-photon shutoff scheme is then

$$c_d^{1S}(i_p) \equiv \max_{\epsilon \in [0,1]} i_d^{1S}(i_p, \epsilon)\,. \tag{27}$$

The maximization in Eq. (27) is numerically performed and plotted in Fig. 5(a), which shows that OOK with single-photon shutoff yields DIE better than standard OOK when the PIE exceeds 2.22 bits/photon, consistent with our earlier result in Eq. (25) that the crossover occurs at an i_p less than 2.885 bits/photon. The performance degradation at low PIE is due to the high mean photon number in this regime. When $\lambda T \gg 1$, most pulses are terminated before the slot duration ends and the information rate is near its ideal limit of 1 bit per channel use. Consequently, the increase in the bandwidth due to the premature termination of the pulse is not matched by an equivalent increase in mutual information, causing a degradation in the DIE relative to standard OOK.

At high PIE, the feedback not only enables higher DIE than otherwise possible with conventional OOK, but also yields a DIE which has the same parametric dependence as the Holevo bound. We show this now by deriving the asymptotic form of c_d^{1S} for PIE$\gg 1$. Again, using the $h_2(\bar{n}) \approx \log_2(e/\bar{n})$ approximation for $\bar{n} \ll 1$, we obtain

$$i_d^{1S} \approx \left(e\, i_p\, 2^{-i_p}\right) \left[\frac{2^{-h_2(\epsilon)}}{d(\epsilon)} \right]. \tag{28}$$

As before, we identify the term in the parenthesis as the asymptotic form of the Holevo bound for $i_p \gg 1$, denoted as c_d^{Hol}. The factor in the square brackets is a function of ϵ but not of the photon efficiency i_p. Thus, the optimal value of ϵ is *independent* of the photon efficiency when $i_p \gg 1$, and it is numerically evaluated to be

$$\epsilon^* = \arg\max_{\epsilon \in [0,1]} 2^{-h_2(\epsilon)} / d(\epsilon) \approx 0.876\,, \tag{29}$$

yielding

$$c_d^{1S}(i_p) \approx 0.274 c_d^{Hol}\,. \tag{30}$$

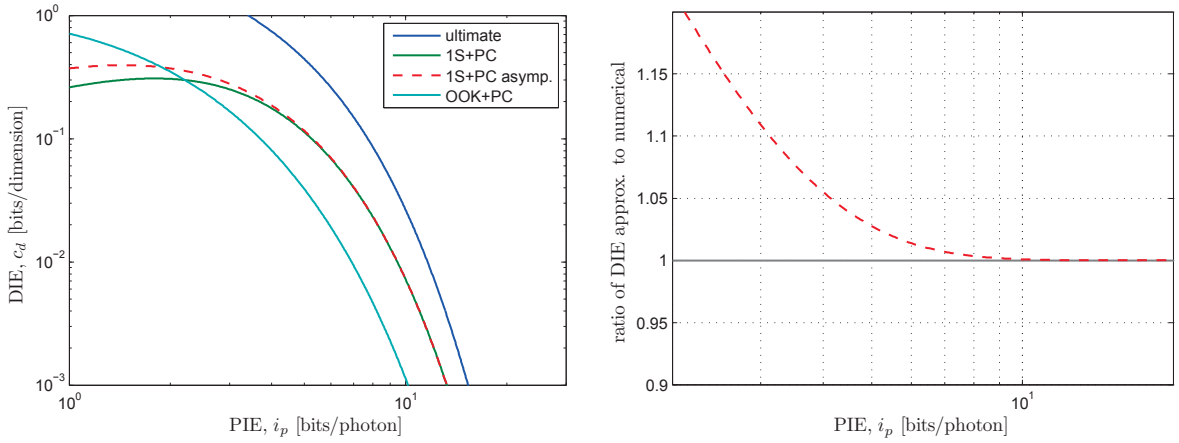

(a) (b)

Figure 5. The numerically-evaluated dimensional information efficiency (DIE) curve for OOK with single-photon shutoff and ideal photon counting (1S+PC), as well as its asymptotic approximation at large photon information efficiency (PIE) are plotted. (a) The numerically-evaluated PIE versus DIE tradeoff curve and its asymptotic approximation. The Holevo bound, and the PIE-DIE curves for conventional OOK with ideal photon-counting (OOK+PC) are also plotted for comparison. (b) The ratio of the asymptotic approximation to the numerically-evaluated DIE.

The ratio of this approximation to the numerically-evaluated DIE is plotted in Fig. 5(b), which shows that the approximation achieves better than 6% accuracy when $i_p > 4\,\text{bits/photon}$. In this regime, the optimal ϵ^* yields an erasure probability of approximately $1-\epsilon^* \approx 0.124$, which corresponds to $\lambda T \approx 2.087$. In other words, the optimal photon flux at high PIE would cost 2.087 photons on average if the transmission continued for the entire symbol duration T. The single-photon shutoff strategy reduces the mean photon cost to $\bar{n} \approx 0.876$ at the expense of an increase in spectral occupancy by a factor of $d(\epsilon^*) \approx 2.383$. The net DIE improvement from this tradeoff, however, is significant. The Eq. (30) approximation reveals that, unlike conventional OOK, the asymptotic dimensional efficiency of OOK with single-photon shutoff has the *same* parametric dependence as the optimal Holevo bound. In particular, its asymptotic DIE is inferior to the ultimate quantum limit by a constant multiplicative factor of 0.274, whereas conventional OOK's asymptotic DIE is inferior to the ultimate quantum limit by a factor that increases linearly in i_p.

5. OOK WITH SINGLE-PHOTON NUMBER-STATES

Recall that the single-mode channel is a beamsplitter of transmissivity η. In the limit that $\eta = 1$, the Holevo capacity can be achieved with a number-state alphabet $\{|n\rangle : n = 0, 1, \dots\}$ (transmitted with a geometric prior probability $p(n) = n_S^n/(1+n_S)^{n+1}$, where n_S is the mean photon number), and an ideal photon-counting receiver.[7] When $n_S \ll 1$, this encoding scheme is well-approximated by a *binary* modulation using the vacuum state $|0\rangle$ and the single-photon number state $|1\rangle$, i.e., the information loss relative to the Holevo capacity, due to the restricted set of modulation states, is small. Although when $\eta < 1$ the information rate of the number-state encoding scheme is strictly inferior to the Holevo capacity, in a near-field communication system wherein $\eta \approx 1$ holds for multiple modes, it is reasonable to expect that this scheme will yield good performance.

Suppose that $|1\rangle$ is chosen with probability p, and $|0\rangle$ is chosen with probability $1-p$. If the transmitter field mode is in the vacuum state, $|0\rangle$, then the output of the beamsplitter is also in a vacuum state. If the transmitter field mode is in the number state $|1\rangle$, then the output field mode is in a mixed state $\eta|1\rangle\langle 1| + (1-\eta)|0\rangle\langle 0|$. Therefore, an ideal photon counting photodetector will yield the following conditional output probabilities:

$$\Pr\big(\text{count} = 1 \big| |1\rangle\text{sent}\big) = \eta \tag{31}$$

$$\Pr\big(\text{count} = 0 \big| |1\rangle\text{sent}\big) = 1-\eta. \tag{32}$$

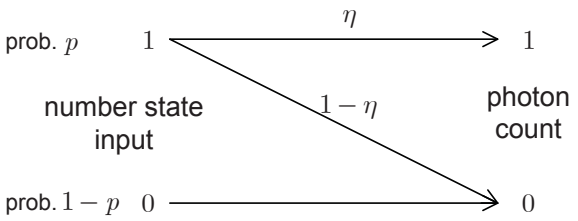

Figure 6. The erasure channel that defines communication with the number-state binary alphabet $\{|0\rangle, |1\rangle\}$.

Thus, once again, we have a Z-channel, but now the erasure probability is $1-\eta$, i.e., it is determined by the channel rather than being a user-optimized parameter. The resultant channel model is illustrated in Fig. 6. We henceforth denote variables pertaining to this architecture with the superscript 1NS.

For a given p and η, the mutual information between the input and the output is given by Eq. (5), but with η replacing ϵ. Therefore, the mutual information per (detected) photon can be written as[§]

$$i_p^{\rm 1NS} = h_2(\bar{n}) - h_2(\eta) \quad \text{bits/photon}, \tag{33}$$

where $h_2(x)$, as before, is the mean derivative of the binary entropy function, and $\bar{n} \equiv p\eta$ is the probability that a photon is counted by the receiver. The corresponding mutual information per dimension is given by

$$i_d^{\rm 1NS} = \bar{n}[h_2(\bar{n}) - h_2(\eta)] \quad \text{bits/dimension}. \tag{34}$$

Note that both $i_p^{\rm 1NS}$ and $i_d^{\rm 1NS}$ are identical to their counterparts in (coherent-state) OOK with single-photon shutoff, but with ϵ replaced by the channel transmissivity η.

In order to evaluate the convex hull of all achievable $(i_p^{\rm 1NS}, i_d^{\rm 1NS})$ pairs with single-photon number-state OOK, we first express $i_d^{\rm 1NS}$, in terms of $i_p^{\rm 1NS}$ and η, as

$$i_d^{\rm 1NS}(i_p, \eta) = h_2^{-1}\big(i_p + h_2(\eta)\big) i_p \,, \tag{35}$$

where we have dropped the superscript of i_p to avoid notation clutter. For a given η value, there are no other parameters in Eq. (35) to be optimized by the user. Hence, we simply define the DIE as $c_d^{\rm 1NS}(i_p;\eta) \equiv i_d^{\rm 1NS}(i_p,\eta)$. Fig. 7(a) plots the resultant PIE versus DIE tradeoff for several values of η. Qualitatively, we observe that the slope of the number-state PIE-DIE curves are better than that of standard OOK, which we will quantitatively confirm shortly. Hence, for every $\eta > 0$, there exists a $i_p^*(\eta)$ value, such that for all $i_p > i_p^*(\eta)$, $c_d^{\rm 1NS}(i_p;\eta) > c_d^{\rm OOK}(i_p)$ holds. However, as η decreases this threshold increases. In particular, empirically we find that at approximately $\eta = 0.1$ the crossover between standard OOK and number-state OOK occurs at 10 bits/photon, and 10^{-3} bits/dimension.

Next, let us derive the asymptotic approximation to $c_d^{\rm 1NS}(i_p)$ for $i_p \gg 1$. In the limit of small $\bar{n} \ll 1$, we have that $h_2(\bar{n}) \approx \log_2(e/\bar{n})$, which implies that

$$c_d^{\rm 1NS}(i_p;\eta) \approx (e i_p 2^{-i_p}) 2^{-h_2(\eta)} \tag{36}$$

$$= c_d^{\rm Hol} 2^{-h_2(\eta)} \tag{37}$$

for $i_p \gg 1$. In Fig. 7(b) we have plotted the ratio of this approximation—at several different η—to the numerically-evaluated DIE curve, which shows excellent agreement. In particular for all η values that we have shown, the accuracy is better than 6%, for $i_p > 4.5$ bits/photon. Therefore, similar to the OOK with single-photon shutoff case, OOK with single-photon number states achieves the *same* parametric dependence as the ultimate PIE-DIE tradeoff, but suffers from a constant penalty factor. However, different from the OOK with

[§]Various normalizations are possible to derive a PIE metric. Here, we have chosen to normalize by the mean number of *detected* photons because it is the most natural metric for the subsequent analysis. Nonetheless, extending the results to other normalizations are straightforward.

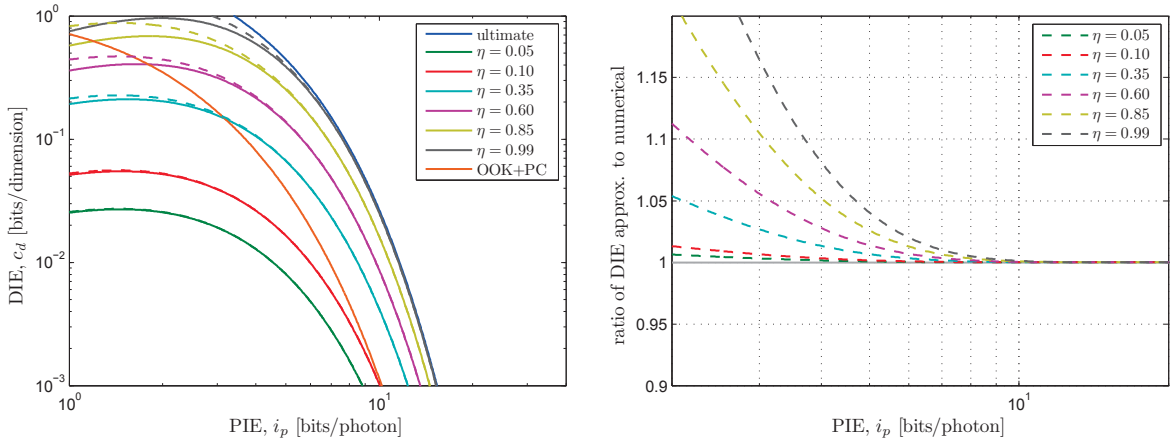

(a) (b)

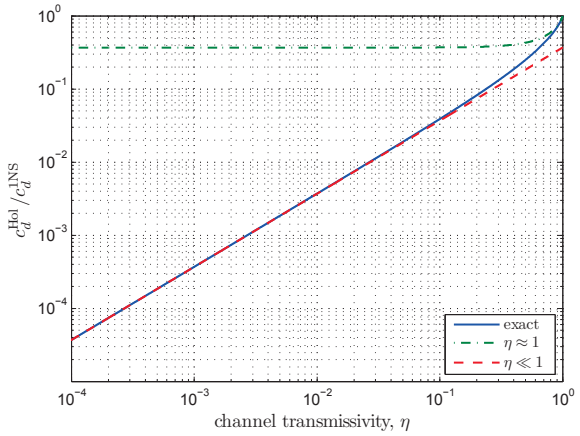

(c)

Figure 7. The numerically-evaluated DIE curve for OOK with single-photon number states and ideal photon counting, as well as its asymptotic approximation at large PIE, are plotted for several different η. (a) The numerically-evaluated PIE versus DIE tradeoff curves (solid lines) and their asymptotic approximations (dashed lines) at different η. The Holevo bound, and the PIE-DIE curves for conventional OOK with ideal photon-counting (OOK+PC) are also plotted for comparison. (b) The ratio of the asymptotic approximations to the numerically-evaluated DIE. (c) The $c_d^{\mathrm{Hol}}/c_d^{\mathrm{1NS}}$ ratio for $i_p \gg 1$, at different η. Dashed (red) line and dash-dotted (green) line denote asymptotic approximations.

single-photon shutoff scheme, the constant penalty factor for OOK with single-photon number states is a function of the channel transmissivity. This factor is equal to $2^{-h_2(\eta)}$, which is approximately equal to $(1-\eta)^{1-\eta}/e^{1-\eta}$ for $\eta \approx 1$, and approximately equal to η/e for $\eta \ll 1$. Figure 7(c) shows the variation of this constant factor as a function of η, along with the aforementioned asymptotes. As a final point of consideration, comparing Eqs. (30) and (37), we find that at $\eta \approx 0.534$, the two schemes achieve the same asymptote for large i_p.

Given that the single-photon number-state OOK modulation is sensitive to the channel losses, it is relevant to briefly discuss typical power coupling that can be achieved in a near-field link geometry. The normal-mode decomposition for hard circular apertures gives rise to Prolate-spheroidal eigenfunctions,[14] and singular values that are not in closed form. This is no longer the case if we replace the hard-pupil apertures of the transmitter and receiver with Gaussian soft apertures.[15] In particular, it can be shown that the input and output eigenfunctions are Laguerre-Gaussian functions, and there are m degenerate eigenvalues equal to $\eta_m = \eta_0^m$ for $m = 1, 2, \ldots$, where

$$\eta_0 = \frac{1 + 2D_F - \sqrt{1 + 4D_F}}{2D_F}\,. \tag{38}$$

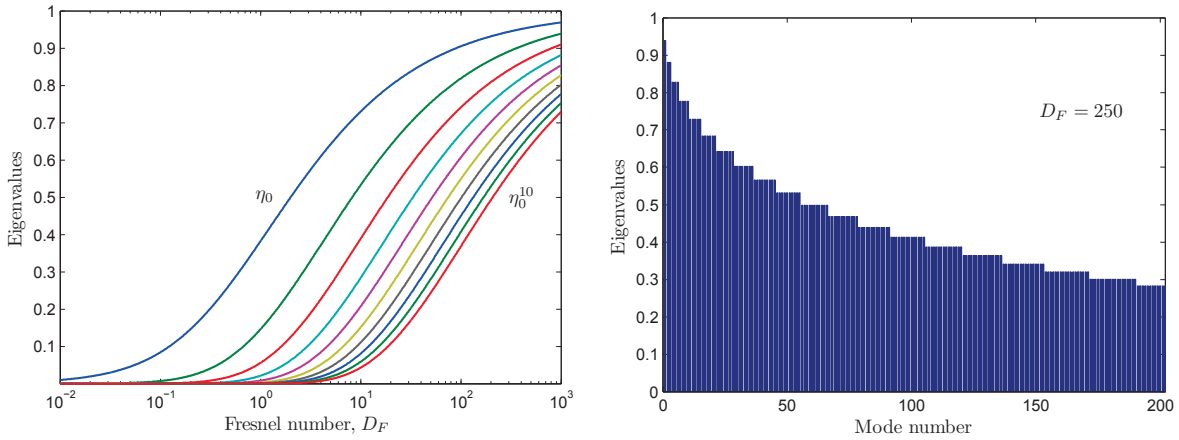

Figure 8. The eigenvalue distribution of a soft-aperture paraxial propagation geometry. (a) Highest 10 distinct eigenvalues as the Fresnel number product varies from the far-field regime ($D_F \ll 1$) to the near-field regime ($D_F \gg 1$); and (b) the eigenvalue distribution—including the repeated eigenvalues—at a fixed near-field Fresnel number $D_F = 250$.

Figure 8(a) plots the growth of the highest 10 *distinct* eigenvalues as a function of D_F, indicating the transition from the far field to the near field regime. Note that the Gaussian soft aperture approximation results in a geometric relationship between distinct eigenvalues, which is less dramatic than what is numerically calculated for hard-pupil apertures.[14,15] In Figure 8(b), we have plotted the eigenvalues of a near-field system with $D_F = 250$. An example of such a geometry is $\lambda_0 = 1\mu$m, $L = 1$km, and equal-size soft Gaussian transmitter and receiver apertures with e^{-1} amplitude attenuation radius equal to 0.1m.[¶] We observe that the first 55 eigenvalues are greater than 0.5, and the top 200 eigenvalues are greater than 0.28.

6. DISCUSSION

Although the maximum rate of reliable communication given a constraint on available resources is the conventional performance metric for a communication system, the performance may be equally characterized in terms of its resource efficiency, i.e., the number of bits that are being (reliably) transmitted per unit of resource that is utilized by the communication system. For bosonic communication systems, the metrics of efficiency can be defined as photon information efficiency (PIE) and dimensional information efficiency (DIE).[5] The ultimate limits of achievable PIE and DIE are determined by the Holevo information bound. This bound can be approached by encoding information in a coherent-state alphabet, which at high PIE is well-approximated by a binary modulation, such as OOK. However, in computing the Holevo information, we implicitly maximize over all possible measurements on the optical codewords generated by this encoding, and only mathematical expressions are known—but not explicit receiver architectures—for the Holevo-bound-achieving measurements. The state of the art of our knowledge in reliable optical communication at high PIE is using generalized OOK (or PPM) in conjunction with photon-counting photodetectors at the receiver. The DIE attained by this scheme (at a given PIE) is inferior to the Holevo ultimate limit, by a factor that *grows* linearly with the PIE, i.e., the DIE of OOK plus photon counting has a suboptimal parametric dependence on PIE, relative to the Holevo bound. Furthermore, recent work has shown that the complexity of receiver architectures grows dramatically even for small gains beyond the PIE-DIE curve attainable with OOK plus ideal photon counting.[5,16]

In this paper, we have approached this problem from the opposite angle, and have begun investigating the ultimate limits achievable *with* a photon-counting receiver, when we allow novel signaling architectures and quantum states tailored to this measurement. Based on insights we have developed in the asymptotic form of

[¶]The Fresnel number product D_F, in Eq. (3), depends on the aperture area. For a soft Gaussian aperture $A(\boldsymbol{\rho}) \equiv e^{-|\boldsymbol{\rho}|^2/r^2}$, where $\boldsymbol{\rho}$ is the 2D spatial coordinate vector on the aperture plane and r is the e^{-1}-attenuation radius, the effective aperture area is given by $\int A^2(\boldsymbol{\rho})\mathrm{d}\boldsymbol{\rho} = \pi r^2/2$.

the PIE-DIE tradeoff for the Holevo limit and standard OOK, we have introduced and analyzed the performance of two novel approaches. We have shown that both of these architectures, at least in theoretical analysis, significantly improve upon the PIE-DIE tradeoff of standard OOK at high PIE values, and furthermore, achieve the *same* parametric dependence as the Holevo bound, so that the performance degradation is asymptotically only a constant factor rather than a factor that grows with PIE.

Although the two approaches we have studied in this paper are promising in their asymptotic performance at high PIE, they bring about their own challenges that may also limit their practicality. Our first approach relies on infinite bandwidth, near-zero latency feedback from the receiver back to a transmitter that is utilizing OOK modulation. We have referred to this system as OOK with single-photon shutoff, as once a photon is detected at the receiver, the feedback is utilized to shut the transmitter off for the remainder of the slot duration, thereby conserving energy that does not carry additional information. The practical challenges associated with this feedback scheme are apparent. First, information cannot travel infinitely fast (even on an ideal feedback channel), thereby limiting the feasibility of this architecture to scenarios where the latency is a small fraction of the slot width. Second, in our analysis the feedback channel has no cost, has infinite bandwidth, and is noiseless. All of these assumptions are too strict for a realistic feedback scenario. Finally, our analysis does not assume that any information other than the shutoff message is being transmitted along the feedback route. It is reasonable to expect that the reverse link carries communication information in addition to the feedback signal. This raises the question of aggregate resource efficiency relative to the (aggregate) Holevo bound of the two channels. While it is apparent that all of these issues are pertinent to realizing a communication system with the feedback, they should not overshadow the underlying fundamental insight offered by this feedback architecture: the asymptotic suboptimality of OOK plus photon-counting in DIE is fundamentally due to energy transmission that does not contribute to information transfer once a photon is detected at the receiver. If the transmitter could shutoff, via some ideal feedback or an oracle, the instant at which the receiver detects the first photon in a slot, the energy conserved from shutting off the transmitter is sufficient to achieve a DIE $c_d^{\mathrm{1S}} = 0.274 c_d^{\mathrm{Hol}}$, which is suboptimal by the constant factor 0.274.

The second approach we have analyzed in this paper is using OOK modulation with number states, $\{|0\rangle, |1\rangle\}$, rather than coherent states. Unlike coherent-state modulation, this architecture inherently pushes the complexity to the transmitter by requiring on-demand generation of a (nonclassical) single-photon number state in a defined spatiotemporal and polarization mode, in addition to requiring efficient transfer of this state from the transmitter to the receiver. Nevertheless, if such a source is available, the DIE is asymptotically $c_d^{\mathrm{1NS}} = 2^{-h_2(\eta)} c_d^{\mathrm{Hol}}$, which is also suboptimal by only a constant factor $2^{-h_2(\eta)}$. This factor now depends on the efficiency, η, with which the number state is transmitted to the photodetector, where η refers to the aggregate efficiency of transmitting a number state, including transmitter optical losses, diffraction loss and absorption, the receiver optical efficiency, and the photodetector quantum efficiency. Although, parametrically this scheme will always perform superior to standard OOK at high enough PIE, the crossover point moves out to higher values of PIE as η degrades. As a rule of thumb, if $\eta > 0.1$, the crossover point is at approximately PIE = 10 bits/photon. Achieving 10% system transmission efficiency, including all of the aforementioned factors, is in general not trivial. However, with improving device technologies it may become feasible to achieve such efficiency values. It is also worthwhile to point out that single-photon number-state generation is an active area of research that has produced several approaches to date, some of which are better suited than others for high-PIE optical communication applications.[17]

To summarize our paper, we have discussed the PIE-DIE tradeoff achievable with 3 communication architectures. First, we revisited generalized OOK with ideal photon counting to introduce our analysis framework and establish the baseline. We showed that the ratio of the maximum DIE determined by the Holevo bound to that achievable with this scheme grows linearly in PIE, establishing that conventional OOK is suboptimal in dimensional efficiency at high PIE. Next, we introduced two new architectures that partially remedy this suboptimality. The OOK with single-photon shutoff scheme utilizes ideal feedback between the receiver and transmitter to terminate a pulse as soon as the first photon is detected by the receiver. We showed that this system is a factor of 0.274 worse than the ultimate DIE, at high PIE. The OOK with single-photon number states scheme utilizes the vacuum state and the $|1\rangle$ number state. We showed that this system is a factor $2^{-h_2(\eta)}$ worse than the ultimate DIE, where η is the end-to-end system efficiency and $h_2(\eta)$ is the mean derivative of the

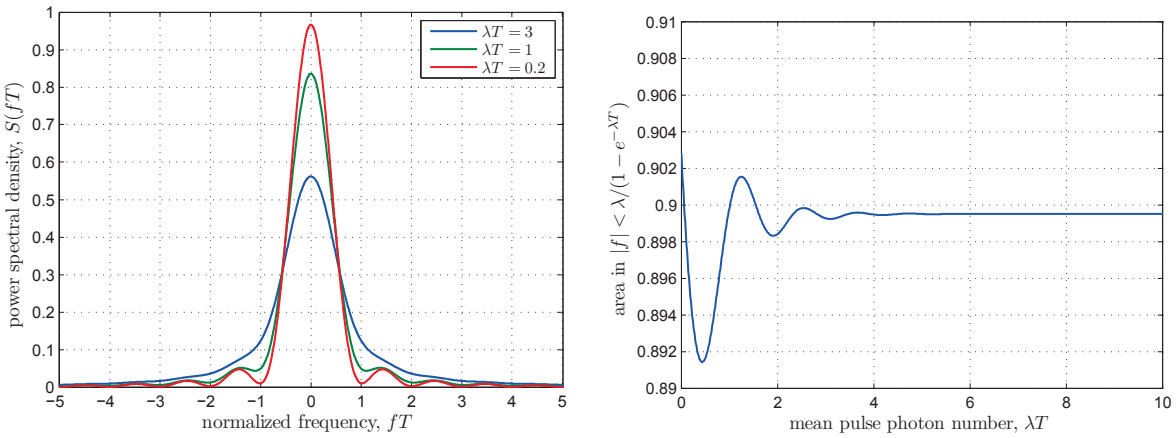

(a) (b)

Figure 9. Power spectral density of OOK with single-photon shutoff assuming $p \ll 1$ such that the delta function contributions from the last term in Eq. (54) are negligible. (a) The power spectral density plotted in terms of the normalized frequency variable fT. (b) The area underneath $S(f)$ for $|f| \leq \lambda/(1-e^{-\lambda T})$.

binary entropy function. Despite having apparent practical challenges, both systems theoretically achieve the exact parametric dependence as the ultimate PIE-DIE tradeoff at high PIE, and only have a constant penalty factor in this regime. Therefore, both systems offer a significant performance improvement over conventional coherent-state OOK modulation at high enough PIE values, and with near-ideal photon-counting photodetectors.

APPENDIX A. POWER SPECTRAL DENSITY FOR OOK WITH SINGLE-PHOTON SHUTOFF

Let $x_N(t)$ denote a sequence of random, real-valued, and integrable pulses over the time interval $-NT < t \leq NT + T$, which we denote as

$$x_N(t) = \sum_{n=-N}^{N} a_n p_{\eta_n}(t - nT)\,, \tag{39}$$

where a_n is a discrete wide-sense stationary (WSS) data sequence, $p_{\eta_n}(t)$, over $0 < t \leq T$, is a nonzero and random pulse shape for the n^{th} symbol, determined by the random variable sequence η_n, which we assume is WSS and independent of a_n.

Suppose $x(t) \equiv \lim_{N\to\infty} x_N(t)$. $x(t)$'s power spectral density can be defined as

$$S(f) \equiv \lim_{N\to\infty} \frac{1}{(2N+1)T} \langle |X_N(f)|^2 \rangle\,, \tag{40}$$

where $X_N(f) \equiv \int_{-NT}^{NT+T} x_N(t) e^{-j2\pi ft} \mathrm{d}t$, and the angled-brackets denote ensemble averaging. Let us define

$$\hat{R}_{x_N}(s) \equiv \mathcal{F}^{-1}\left\{ \frac{1}{(2N+1)T} |X_N(f)|^2 \right\} = \frac{1}{(2N+1)T} \int_{-NT}^{NT+T} x_N(t) x_N(t-s) \mathrm{d}t\,, \tag{41}$$

where $\mathcal{F}$ denotes the Fourier transform and $\mathcal{F}^{-1}$ its inverse. We then have $S(f) \equiv \lim_{N\to\infty} \langle \mathcal{F}\{\hat{R}_{x_N}(s)\} \rangle$. Substituting Eq. (39) in the expression above, we obtain

$$\hat{R}_{x_N}(s) = \frac{1}{(2N+1)T} \sum_{n=-N}^{N} \sum_{m=-N}^{N} a_n a_m \int_{-\infty}^{\infty} p_{\eta_n}(t - nT - s) p_{\eta_m}(t - mT) \mathrm{d}t\,, \tag{42}$$

where we have extended the limits of the integral to infinity because of our assumption that the pulses $p_{\eta_n}(t)$ are zero everywhere outside of $0 < t \leq T$. For a given random variable η, we define $P_\eta(f) \equiv \mathcal{F}\{p_\eta(t)\}$, such that

$$\hat{R}_{x_N}(s) = \frac{1}{(2N+1)T} \sum_{n=-N}^{N} \sum_{m=-N}^{N} a_n a_m \int_{-\infty}^{\infty} P^*_{\eta_n}(f) P_{\eta_m}(f) e^{j2\pi(n-m)fT} e^{j2\pi fs} \mathrm{d}f \,. \tag{43}$$

Now, we take the expectation of both sides in Eq. (43). Recalling that $\{a_n\}$ and $\{\eta_n\}$ are WSS independent sequences, we obtain

$$\left\langle \hat{R}_{x_N}(s) \right\rangle = \frac{1}{T} \sum_{\ell=-2N}^{2N} \left(1 - \frac{|\ell|}{2N+1}\right) \langle a_\ell a_0 \rangle \int_{-\infty}^{\infty} \left\langle P^*_{\eta_\ell}(f) P_{\eta_0}(f) \right\rangle e^{j2\pi\ell fT} e^{j2\pi fs} \mathrm{d}f \tag{44}$$

where $\ell = n + m$, and $1 - \frac{|\ell|}{2N+1}$ is a Bartlett function. If the expression

$$\sum_{\ell=-\infty}^{\infty} |\ell| \langle a_\ell a_0 \rangle \int_{-\infty}^{\infty} \left\langle P^*_{\eta_\ell}(f) P_{\eta_0}(f) \right\rangle e^{j2\pi\ell fT} e^{j2\pi(f-f')s} \mathrm{d}f \tag{45}$$

is bounded for all $s \in \mathbb{R}$ and $f' \in \mathbb{R}$, then the Fourier transform and the limit operations can be exchanged in deriving $S(f)$. With this assumption, we have

$$R_x(s) \equiv \mathcal{F}^{-1}\{S(f)\} = \lim_{N\to\infty} \left\langle \hat{R}_{x_N}(s) \right\rangle \tag{46}$$

$$= \frac{1}{T} \sum_{\ell=-\infty}^{\infty} \langle a_\ell a_0 \rangle \int_{-\infty}^{\infty} \left\langle P^*_{\eta_\ell}(f) P_{\eta_0}(f) \right\rangle e^{j2\pi\ell fT} e^{j2\pi fs} \mathrm{d}f \,, \tag{47}$$

which yields,

$$S(f) = \frac{1}{T} \sum_{\ell=-\infty}^{\infty} \langle a_\ell a_0 \rangle \left\langle P^*_{\eta_\ell}(f) P_{\eta_0}(f) \right\rangle e^{j2\pi\ell fT} \,. \tag{48}$$

As a final step, assuming that the random sequences $\{a_\ell\}$ and $\{\eta_\ell\}$ are identically distributed, we arrive at

$$S(f) = \frac{1}{T} \left\{ \left[\left\langle |a_0|^2 \right\rangle \left\langle |P_\eta(f)|^2 \right\rangle - |\langle a_0 \rangle|^2 |\langle P_\eta(f) \rangle|^2 \right] + |\langle a_0 \rangle|^2 |\langle P_\eta(f) \rangle|^2 \sum_{k=-\infty}^{\infty} \delta(fT - k) \right\} . \tag{49}$$

We can now apply this result to the Section 4 modulation waveform. Recall that in the single-photon shutoff scheme we transmit a pulse of photon flux λ with probability p and no pulse (photon flux 0) with probability $1 - p$. The receiver shuts off the transmitter, via feedback, once a photon is received. This implies that a_n is an independent, identically distributed sequence with $\Pr(a_n = 1) = p$, and $\Pr(a_n = 0) = 1 - p$. The pulse $p_\tau(t)$ is a rectangular pulse with amplitude λ, and random duration τ, such that $p_\tau(t) = \lambda$ for $0 < t \leq \tau$, and zero otherwise. The Fourier transform of $p_\tau(t)$ is given by

$$P_\tau(f) = \int_0^\tau \lambda e^{-j2\pi fs} \mathrm{d}s = \frac{\lambda}{j2\pi f} \left(1 - e^{-j2\pi f\tau}\right) , \tag{50}$$

which yields

$$\langle P_\tau(f) \rangle = \frac{\lambda}{j2\pi f} \big(1 - G(f)\big) \,, \tag{51}$$

and

$$\left\langle |P_\tau(f)|^2 \right\rangle = \frac{\lambda^2}{(2\pi f)^2} \big(2 - G(f) - G^*(f)\big) \,, \tag{52}$$

where

$$G(f) \equiv \left\langle e^{-j2\pi f\eta} \right\rangle = \frac{\lambda + j2\pi f e^{-(\lambda + j2\pi f)T}}{\lambda + j2\pi f} \,. \tag{53}$$

Substituting Eqs. (51)–(53) into (49) , we arrive at the power spectral density for OOK with single-photon shutoff:

$$S(f) = p\lambda^2 T \left\{ 2\frac{1 - \lambda T e^{-\lambda T}\mathrm{sinc}(2\pi fT) - e^{-\lambda T}\cos(2\pi fT)}{(\lambda T)^2 + (2\pi fT)^2} - p\frac{1 - 2e^{-\lambda T}\cos(2\pi fT) + e^{-2\lambda T}}{(\lambda T)^2 + (2\pi fT)^2} \right.$$
$$\left. + p\left(1 - e^{-\lambda T}\right)^2 \sum_{k=-\infty}^{\infty} \frac{1}{(\lambda T)^2 + (2\pi fT)^2}\delta(fT - k) \right\}, \quad (54)$$

where $\mathrm{sinc}(x) \equiv \sin(x)/x$. In Fig. 9(a) we have plotted this power spectral density for various λT, assuming $p \ll 1$ such that the latter two terms in Eq. (54) are negligible. This assumption is valid when PIE $\gg 1$. In Fig. 9(b) we have plotted the mean photon flux contained in $|f| < \lambda/(1-e^{-\lambda T})$ as a function of λT, which shows that to a very good approximation 90% of the total mean photon flux is contained within this frequency band.

ACKNOWLEDGMENTS

This research was supported by the DARPA InPho program under contract number JPL 97-15402, and was carried out by the Jet Propulsion Laboratory, California Institute of Technology, under a contract with the National Aeronautics and Space Administration.

REFERENCES

1. M. A. Nielsen and I. L. Chuang, *Quantum Computation and Quantum Information*, Cambridge Univ., Cambridge, 2000.
2. A. S. Holevo, "The capacity of the quantum channel with general signal states," *IEEE Trans. Inform. Theory* **44**, pp. 269–273, 1998.
3. P. Hausladen, R. Jozsa, B. Schumacher, M. Westmoreland, and W. K. Wooters, "Classical information capacity of a quantum channel," *Phys. Rev. A* **54**, pp. 1869–1876, 1996.
4. S. Guha, "Structured optical receivers to attain superadditive capacity and the Holevo limit," *Phys. Rev. Lett.* **106**, art. 240502, 2011.
5. S. Dolinar, K. M. Birnbaum, B. I. Erkmen, and B. Moision, "On approaching the ultimate limits of photon-efficient and bandwidth-efficient optical communication," *Space Optical Systems and Applications (ICSOS), 2011 International Conference on* , pp. 269–278, 2011.
6. B. I. Erkmen, K. M. Birnbaum, B. E. Moision, and S. J. Dolinar, "The Dolinar receiver in an information theoretic framework," *Proc. SPIE* **8163**, art. 81630U, 2011.
7. H. P. Yuen and M. Ozawa, "Ultimate information carrying limit of quantum systems," *Phys. Rev. Lett.* **70**, pp. 363–366, 1993.
8. S. Verdú, "On channel capacity per unit cost," *IEEE Trans. Inform. Theory* **36**, pp. 1019–1030, 1990.
9. J. H. Shapiro, "The quantum theory of optical communications," *IEEE J. Sel. Top. Quantum Electron.* **15**, p. 1547, 2009.
10. J. H. Shapiro, "Corrections to 'The quantum theory of optical communications' [Nov/Dec 09 1547-1569]," *IEEE J. Sel. Top. Quantum Electron.* **16**, p. 698, 2010.
11. J. H. Shapiro, "Normal-mode approach to wave propagation in the turbulent atmosphere," *Appl. Opt.* **13**, pp. 2614–2619, 1974.
12. B. I. Erkmen, B. E. Moision, and K. M. Birnbaum, "A review of the information capacity of single-mode free-space optical communication," *Proc. SPIE* **7587**, art. 75870N, 2010.
13. V. Giovannetti, S. Guha, S. Lloyd, L. Maccone, J. H. Shapiro, and H. P. Yuen, "Classical capacity of the lossy bosonic channel: The exact solution," *Phys. Rev. Lett.* **92**, art. 027902, 2004.
14. D. Slepian, "Analytic solution of two apodization problems," *J. Opt. Soc. Am.* **55**, pp. 1100–1115, 1965.
15. J. H. Shapiro, S. Guha, and B. I. Erkmen, "Ultimate channel capacity of free-space optical communications [invited]," *J. Opt. Netw.* **4**, pp. 501–516, 2005.
16. S. Guha, Z. Dutton, and J. H. Shapiro, "On quantum limit of optical communications: concatenated codes and joint-detection receivers," *IEEE International Symposium on Information Theory (ISIT)*, 2011.
17. M. D. Eiseman, J. Fan, A. Migdall, and S. V. Polyakov, "Invited review article: Single-photon sources and detectors," *Rev. Sci. Instrum.* **82**, art. 071101, 2011.